Ecotoxicology and Environmental Safety 145 (2017) 349–358

Contents lists available at ScienceDirect

Ecotoxicology and Environmental Safety

journal homepage: www.elsevier.com/locate/ecoenv

Importance of exposure dynamics of metal-based nano-ZnO, -Cu and -Pb governing the metabolic potential of soil bacterial communities

Yujia Zhai[a,*], Ellard R. Hunting[a], Marja Wouterse[b], Willie J.G.M. Peijnenburg[a,b], Martina G. Vijver[a]

[a] Institute of Environmental Sciences (CML), Leiden University, P.O. Box 9518, 2300 RA, Leiden, The Netherlands
[b] National Institute of Public Health and the Environment (RIVM), P.O. Box 1, Bilthoven, The Netherlands

ARTICLE INFO

Keywords:
Engineered nanomaterials
Nano-ecotoxicity
Dynamic exposure
Relative contribution
Bacterial catabolic potential

ABSTRACT

Metal-based engineered nanomaterials (ENMs) are known to affect bacterial processes and metabolic activities. While testing their negative effects on biological components, studies traditionally rely on initial exposure concentrations and thereby do not take into consideration the dynamic behavior of ENMs that ultimately determines exposure and toxicity (e.g. ion release). Moreover, functional responses of soil microbial communities to ENMs exposure can be caused by both the particulate forms and the ionic forms, yet their relative contributions remain poorly understood. Therefore, we investigated the dynamic changes of exposure concentrations of three different types of ENMs (nano-ZnO, -Cu and -Pb) and submicron particles (SMPs) in relation to their impact on the capacity of soil bacterial communities to utilize carbon substrates. The different ENMs were chosen to differ in dissolution potential. The dynamic exposures of ENMs were considered using a time weighted average (TWA) approach. The joint toxicity of the particulate forms and the ionic forms of ENMs was evaluated using a response addition model. Our results showed that the effect concentrations of spherical nano-ZnO, -Cu and SMPs, and Pb-based perovskites expressed as TWA were lower than expressed as initial concentrations. Both particulate forms and ionic forms of spherical 18 nm, 43 nm nano-ZnO and 50 nm, 100 nm nano-Cu contribute to the overall response at the EC_{50} levels. The particulate forms for 150 nm, 200 nm and 900 nm ZnO SMPs and rod-shaped 78 nm nano-Cu mainly affected the soil microbial metabolic potential, while the Cu ions released from spherical 25 nm nano-Cu, 500 nm Cu SMPs and Pb ions released from perovskites mainly described the effects to bacterial communities. Our results indicate that the dynamic exposure of ENMs and relative contributions of particles and ions require consideration in order to pursue a naturally realistic assessment of environmental risks of metal-based ENMs.

1. Introduction

Metal-based engineered nanomaterials (ENMs) have been widely applied in various medical, industrial and environmental applications (Wang et al., 2016). Given the wide and increasing use of ENMs, they are likely to ultimately end up in the soils and sediments through wastewater effluents and deposition (Shah and Belozerova, 2009), and hence warrants an understanding of emerging hazards and risks (McKee and Filser, 2016).

ENMs are known to affect bacteria (Du et al., 2015), to inhibit bacterial metabolic activities and hence their ability to utilize available carbon resources (Echavarri-Bravo et al., 2015; Sillen et al., 2015). Toxicity of ENMs, however, can be changed by the physico-chemical properties like metal type, shape, size, dissolution and stability/aggregation. The fate of ENMs in the natural environment depends on a plethora of variables that affect dissolution behaviors of ENMs (e.g. pH, natural organic matter, temperature, electrolyte), and these variables can be spatially and temporally highly heterogeneous (Topuz and van Gestel, 2015). Dissolution in various environmentally relevant media is reported in the range of 1–80% for nano-Cu, and nano-ZnO ENMs, which highlights the importance of thorough and exposure-specific characterization during experiments (Misra et al., 2012). The use of the time weighted average concentrations (C_{TWA}) has therefore been proposed to offer a more environmentally realistic display for exposure concentrations compared to using initially measured concentrations (C_I). This approach has gained interest for risk assessment of degradable compounds such as many pesticides (Belgers et al., 2011), and was recently also explored for ENMs that show time-variable exposure, e.g. silver nanoparticles (Zhai et al., 2016). However, it remains uncertain how the dynamic behavior of ENMs exposure affects the expression of

* Corresponding author.
E-mail address: y.zhai@cml.leidenunv.nl (Y. Zhai).

http://dx.doi.org/10.1016/j.ecoenv.2017.07.031
Received 12 June 2017; Received in revised form 11 July 2017; Accepted 15 July 2017
Available online 28 July 2017

toxicity (Meesters et al., 2013), in particular in comparison to static or semi-static concentrations and in relation to the metabolic or functional potential of soil bacterial communities.

A key attribute of suspensions of metal-based ENMs is that both particles and ions shedding from ENMs contribute to the overall toxicity (Hua et al., 2014). It is already known that the toxicity caused by nanoparticles cannot be simply explained by the metal ions released from the nanoparticles into the exposure medium (Karlsson et al., 2008). Moreover, the relative contributions of the particulate forms and the ionic forms to the overall toxicity of ENMs and SMPs have been observed to differ between metal species and the organisms under focus. Predominantly, particle specific toxicity of nano-Cu and nano-ZnO has been observed for *Ceriodaphnia dubia* (Bhuvaneshwari et al., 2016), *Daphinia magana* (Santo et al., 2014), and various cell lines e.g. rat hepatoma (H4IIE) and human hepatocellular carcinoma (HepG2) (Song et al., 2014), while the ions released from nano-Ag appears more toxic to microorganisms (Ivask et al., 2014). This highlights the importance to determine the relative contributions of the particulate forms and the ionic forms of ENMs and SMPs to the overall toxicity at a community level.

This study therefore aims to: 1) investigate the dynamic exposure accounting for time-variable concentrations of metal-based ENMs and their impact on the capacity of soil to utilize environmentally relevant carbon sources, 2) determine the relative toxic contributions of the ionic forms versus the particulate forms of ENMs. To this end, we evaluated the effect of three different types of metal-based ENMs (nano-ZnO, -Cu, -Pb and submicron particles (SMPs)) with different sizes and shapes on the metabolic potential of soil bacterial communities by assessing their ability to utilize a distinct set of carbon substrates in simplified laboratory incubations.

2. Materials and methods

2.1. Nanomaterials and characterizations

Three different types of ENMs (nano-Cu, -Pb and -ZnO) and SMPs were tested, as described in Table A.1. Characterizations of the particle morphology of ENMs and SMPs were performed using transmission electron microscopy (TEM) (JEOL 1010, IEOL Ltd., Japan). The size distribution and zeta potential of suspensions of ENMs and SMPs were analyzed at 1 and 96 h incubation in the exposure medium using dynamic light scattering (DLS) on a zetasizer Nano-ZS instrument (Malvern, Instruments Ltd., UK). Metal salts $Zn(NO_3)_2{\cdot}6H_2O$, $CuCl_2{\cdot}2H_2O$, and $PbCl_2$ were purchased from Sigma-Aldrich (Zwijndrecht, The Netherlands).

2.2. Dissolution behaviors of ENMs and SMPs

The release profiles of soluble Zn, Cu and Pb species released from the ENMs and SMPs at 1 mg/L for 96 h were investigated. ENMs and SMPs suspensions were sampled at 1, 24, 48, 72 and 96 h and centrifuged at 30392 g for 30 min at 4 °C (Sorvall RC5Bplus centrifuge, Fiberlite F21-8 × 50 y rotor; Hua et al., 2014; Song et al., 2014; Xiao et al., 2015) to remove (aggregated) ENMs and SMPs. After centrifugation, the supernatant was filtered through a syringe filter with 0.02 μm pore diameter (Anotop 25, Whatman, Xiao et al., 2015). The supernatants were continually confirmed using DLS that (aggregated) ENMs and SMPs were removed. Subsequently, the concentrations of the ENMs and SMPs suspensions and the corresponding soluble Zn, Cu and Pb species in the supernatants were measured by inductively coupled plasma optical emission spectrometry (ICP-OES) after digestion in 65% HNO_3 solutions with final concentrations of 5 v/v% HNO_3 (Xiao et al., 2015).

2.3. Bacterial community

Soil bacterial community extracts were collected from the top 15 cm of a soil (52°07'06.7"N 5°11'23.1"E, site dominated by deciduous trees, The Netherlands) as described previously (Zhai et al., 2016). In brief, collected soils were sieved through an 8 mm sieve. Soil water hold capacity was 17.5%. After soil collection, the soil samples were stored at 4 °C before the experiments. Subsequently, distilled water was added to maintain the soil moisture content at 18.4% of the dry soil weight and pre-incubated for 3–4 weeks at 10 °C (Bloem and Bolhuis, 2006). During the experiments, soil samples were diluted 10 times with 10 mM BIS-TRIS buffer (Sigma-Aldrich B9754, 2.09 g/L, pH = 7; Rutgers et al., 2016). The diluted soil samples were then centrifuged at 1500 rpm for 10 min (Rutgers et al., 2006). The supernatant was then diluted 5 times using the same buffer to obtain the soil bacterial community extract.

2.4. Substrates utilizations by soil bacterial community

The utilizations of environmentally relevant substrates were determined using commercial Ecoplates (Biolog, Hayward, USA). The Biolog Ecoplate contains 31 of the most useful carbon substrates (see Table A.2), replicated 3 times (Garland and Mills, 1991). Each well of the Ecoplate contains a single carbon substrate and a tetrazolium that turns purple upon microbial respiration and dehydrogenation of the respective carbon source.

There are many limitations to this method. It is confined to a culturable fraction of the microbial community for which tetrazolium is not toxic (Stefanowicz, 2006), and Ecoplates also do not include e.g. recalcitrant substrates nor specific substrates typical of the soils used in this study (Hunting et al., 2013). The different request of nutrient and complicated interactions between bacterial species hamper identification of the microorganisms contributing to substrates utilization. It is thus impossible to directly relate the carbon substrates utilization to actual microbial community structure and how they would function under natural conditions, yet the number of utilized substrates offers a proxy of the functional diversity or metabolic potential of a microbial community (Schutter and Dick, 2001; Hunting et al., 2015; Echavarri-Bravo et al., 2015). However, molecular approaches to study microbial diversity requires scarifying individual samples, thereby hampering studying the temporal aspects of microbial community dynamics. Thus, despite its limitations, Biolog offers the unique opportunity to track changes in the metabolic potential in relation to the dynamic changes of ENM-exposure.

2.5. Experimental outline

Suspensions of ENMs and SMPs were prepared following the Risk Assessment of Engineered Nanoparticles (ENPRA) protocol for toxicological studies (Kermanizadeh et al., 2012). The stock suspensions (nominal 100 mg/L) of each ENM and SMP were sonicated in a water bath sonicator in 4 °C water at 38 ± 10 kHz (twice, 8 min each, shaked in between). Thereafter, several identical sets of ENMs and SMPs suspensions were prepared immediately by a series of dilution from the stock solution with buffer. The soil bacterial community extract was added to different treatments with ENMs and SMPs suspensions, and the negative control treatment consisting of soil extract dosed with buffer instead of ENMs solution. The effects of $Zn(NO_3)_2{\cdot}6H_2O$, $CuCl_2{\cdot}2H_2O$, and $PbCl_2$ were tested as a positive treatment to assess the toxicity of Zn(II), Cu(II) and Pb(II). Measured exposure ranges of ENMs and SMPs suspensions are listed in Table 1. To enhance bacterial growth, 100 μl of the soil bacterial community extract mixed with ENMs and SMPs suspensions were incubated in each well of the Ecoplates for 96 h at 20 °C. Optical density was measured at 590 nm (OD_{590}) at every 24 h during the incubation to ensure saturation of the substrates utilization. The final calculations were performed based on the 96 h measurement (Sillen et al., 2015). The ENMs and SMPs

Table 1
The EC_{50} values of the total and particulate forms of ENMs and SMPs using the RA model expressed in terms of initial concentrations (C_I) or 96 h time weighted average concentration (C_{TWA}) of particulate forms of ENMs and SMPs.

Element	Size and shape	Exposure range (mg/L)	EC_{50} (mg/L)		
			ENMs and SMPs (total)	ENMs and SMPs (particle)	
				C_{TWA}	C_I
Zn	18 nm spheres[a]	0.16–12.88	1.34	1.07*	1.38*
	43 nm spheres[a]	0.26–12.30	1.51	1.52*	1.80*
	150 nm rods[b]	0.12–15.14	1.65	1.80	1.91
	200 nm cubes[b]	0.15–12.59	1.74	1.98	2.06
	900 nm cubes[b]	0.13–13.49	1.99	2.09	2.17
Cu	25 nm spheres[a]	0.11–1.66	0.30	0.28*	0.57*
	50 nm spheres[a]	0.14–1.86	0.38	0.36*	0.64*
	78 nm rods[a]	0.25–7.94	0.57	0.74	0.81
	100 nm spheres[a]	0.15–5.62	0.54	0.56*	0.84*
	500 nm spheres[b]	0.12–2.92	0.39	0.45*	0.78*
Pb	100 nm hexagon[a]	0.71–67.52	7.54	25.31*	46.15*
	150 nm hexagon[b]	0.45–53.25	9.36	45.72*	68.56*
	400 nm hexagon[b]	1.13–89.13	13.31	53.61*	72.55*
	500 nm hexagon[b]	1.30–95.82	14.57	74.57*	93.15*

* Independent sample test was used to detect significant differences between EC_{50} values based on C_I and C_{TWA} for each metal species separately. $p < 0.05$ is statistically significant.
[a] Nano particles (ENMs).
[b] Submicron particles (SMPs).

suspensions are composed of the particulate forms and the soluble ionic metal species (ionic forms) of ENMs and SMPs. During the incubation, the ENMs and SMPs suspensions of each treatment were also sampled at 1, 24, 48, 72 and 96 h and centrifuged at 30,392 g for 30 min to obtain the soluble ionic metal species of ENMs and SMPs in the supernatants. The concentrations of suspensions and supernatant, as well as Zn $(NO_3)_2{\cdot}6H_2O$, $CuCl_2{\cdot}2H_2O$, and $PbCl_2$, were determined using ICP-OES after digestion in 65% HNO_3 solutions with final concentrations of 5 v/v% HNO_3. The concentrations of the particulate forms of ENMs and SMPs were derived by the difference between the metal concentrations measured in the suspensions and the metal concentrations measured in the supernatants.

2.6. Data analysis

2.6.1. Average well color development (AWCD)

Average well color development (AWCD) was used to represent the average bacterial metabolic activity. AWCD is calculated for the 31 substrates of the wells. OD_0 is the OD_{590} for blank well and OD_k is the OD_{590} for well k according to the following equation (Garland and Mills, 1991):

$$AWCD = \frac{1}{31}\sum_{i=1}^{31}(OD_k - OD_0) \quad (1)$$

The data for any Ecoplate was initially normalized by the AWCD value. The normalized absorbance for well k was calculated using the following equation:

$$\overline{OD_k} = \frac{OD_k - OD_0}{\frac{1}{31}\sum_{i=1}^{31}(OD_k - OD_0)} \quad (2)$$

A natural logarithmic transformation was used according to the following equation (Weber et al., 2007):

$$OD' = \ln(\overline{OD_k}+1) \quad (3)$$

The transformed values of OD_k greater than 0.25 were chosen to reflect positive response to the substrates utilizations (Sillen et al., 2015).

2.6.2. Time weighted average approach (TWA)

The TWA concentrations of the particulate forms of ENMs and SMPs at 1, 24, 48, 72 and 96 h were calculated according to the following equation (Belgers et al., 2011):

$$C_{TWA} = \frac{\sum_{n=1}^{N}\left(\Delta t_n \frac{c_{n-1}+c_n}{2}\right)}{\sum_{n=1}^{N}\Delta t_n} \quad (4)$$

Where Δt is the time interval, n is the time interval number, N is the total number of intervals (N = 4), c is the concentration at the end of the time interval.

2.6.3. Dose-response model

The median effect concentration (EC_{50}) of AWCD inhibition of soil bacterial communities caused by ENMs and SMPs was calculated according to the dose-response curve (Hua et al., 2014):

$$E = \frac{1}{1+10^{(LogEC_{50}-LogC)\rho}} \quad (5)$$

Where E is the effect (AWCD inhibition) on soil bacterial communities caused by ENMs and SMPs (scaled from 0 to 1), C is the exposure concentration of ENMs and SMPs and ρ is the slope of the curve. The EC_{50} values and ρ for the suspensions and particulate forms of ENMs and SMPs are listed in Table A.4. The EC_{50} values and ρ $Zn(NO_3)_2{\cdot}6H_2O$, $CuCl_2{\cdot}2H_2O$, and $PbCl_2$ for the are listed in Table A.5.

2.6.4. Contribution of particulate forms and ionic forms of ENMs and SMPs to overall response

Generally, species are exposed to mixtures of different substances instead of a single substance in the environment. The concentration addition (CA) model and the response addition (RA) model are common models to predict the joint effects of chemicals based on the effect of the individual chemical present in a mixture. The CA model is used to predict a similar mode of action (non-interactive joint action) of a mixture of compounds. The independence of the mode of action thus has a tendency to be conservative (Gregorio et al., 2013). It is likely that the mode of action of metal ions differs from that of the metal-based ENMs (Ivask et al., 2014; Boudreau et al., 2016). The ENMs suspension is a mixture of soluble metal ionic species released from ENMs and particulate forms, and all the dissolved metal species are assumed to be in the ionic forms of ENMs. To calculate the individual contributions of particulate forms and ionic forms of ENMs and SMPs, we therefore assumed that the mode of action of particulate forms is dissimilar with the mode of action of the ionic forms, which is in line with the assumption of response addition (RA) model. The effect of the particulate

forms of ENMs and SMPs were included in the RA model using the following equation (Backhaus et al., 2000):

$$E_{(total)} = 1-((1 - E_{(ion)})(1 - E_{(particle)})) \quad (6)$$

Where $E_{(total)}$, $E_{(ion)}$ and $E_{(particle)}$ represent the effects caused by the nanoparticle suspensions, their corresponding released ions and the corresponding particulate forms, respectively. In the present study, $E_{(total)}$ was measured by the AWCD of the suspensions experimentally; $E_{(ion)}$ was calculated according to the concentration-response curve of $Zn(NO_3)_2{\cdot}6H_2O$, $CuCl_2{\cdot}2H_2O$, and $PbCl_2$ towards AWCD. This makes $E_{(particle)}$ as the only unknown, allowing for direct calculation of the effects caused by the particulate forms of ENMs and SMPs.

The exposures were performed using 3 replicates of aliquots of the same diluted soil extract. The dose-response models were used to calculate the EC_{50} values for the total and the particulate forms of ENMs and SMPs using GraphPad Prism 6.0. Statistically significant differences between soil bacterial community extracts exposed to different ENMs and SMPs treatments were determined by means of a two-way ANOVA and Tukey's honestly significant difference tests (with significance level set as $p < 0.05$) using SPSS 16.0. The carbon substrates utilizations under treatments with different ENMs and SMPs were analyzed using a Euclidean-based cluster analysis and a one-way analysis of similarities (ANOSIM) using PAST 3.0 to determine the bacterial functional composition (Hammer et al., 2001; Villéger et al., 2008). The carbon substrates utilizations under treatments with different ENMs and SMPs were also assessed by principal component analysis (PCA) and heatmap analysis (supplementary data). The carbon substrates included in the PCA and heatmap showed a net OD > 0.25, indicating substrate utilization.

3. Results

3.1. Physico-chemical characterization of ENMs and SMPs

The transmission electron microscopic images of different shaped and sized ENMs and SMPs in the buffer are shown in Fig. 1. Data on size distributions and zeta potential after 1 and 96 h incubation in the buffer are given in Table A.3. The results revealed that the particles used in this study were spherical, rod, cuboidal and hexagonal particles. After being suspended in the incubation media, the particles are present largely in aggregates, except for the spherical 500 nm Cu SMPs, which had rough edged appearance and the size decreased dramatically.

3.2. Dissolution behaviors of ENMs and SMPs

The concentrations of the ionic forms of ENMs and SMPs dissolved from the ENMs and SMPs are shown in Fig. 2 (A-C). The overall trend observed was that dissolution appeared to be occurring at a greater rate in the first two time intervals and then levels off after 80 h. The relative amounts of dissolved Zn ions were different for differently shaped and sized nano-ZnO, with spherical 18–43 nm nano-ZnO releasing more Zn ions (38–45%), whereas only 12–17% of Zn ions released from cuboidal 200–900 nm ZnO SMPs (Fig. 2A). There was a higher Cu ion release percentage of spherical nano-Cu than in case of the rod-shaped particles. The spherical 50 and 100 nm nano-Cu showed similar ion release percentages (21–24%). Approximately 33% of 25 nm nano-Cu and 43% of the 500 nm Cu SMPs were dissolved after 96 h. The 78 nm rod-shaped nano-Cu showed the lowest ion release rate (14%) among all suspensions (Fig. 2B). The release of Pb ions from 100 and 150 nm hexagonal-shaped perovskites were similar and yielded ion release percentages of 75–78%, while 400 and 500 nm hexagonal-shaped perovskites display lower ion release percentages of 50–57% at 96 h (Fig. 2C). It was also showed that smaller particles of nano-ZnO and SMPs, nano-Cu and perovskites releasing higher amount of ions. This could be explained by the largest net surface area; however, the 500 nm Cu SMPs released more Cu ions than 78 nm nano-Cu, which was due to the smaller particle size of Cu SMPs suspended in the media according to the TEM observation.

Based on the measured total exposure concentrations and ion release profiles of ENMs and SMPs, the concentrations of the particulate forms during 96 h of incubation in the exposure medium are presented in Fig. 2 (D-F). The results illustrate that the exposure concentrations for all the particulate form of ENMs and SMPs decreased along with time depending on the shapes and sizes of ENMs and SMPs. For the spherical 18–43 nm nano-ZnO, concentrations of the particulate Zn after 96 h incubation were 8–10% less than the initial concentrations, while slight differences were found in the Zn concentrations of 150–900 nm ZnO $SMPs_{(particle)}$ along with time (Fig. 2D). After 96 h

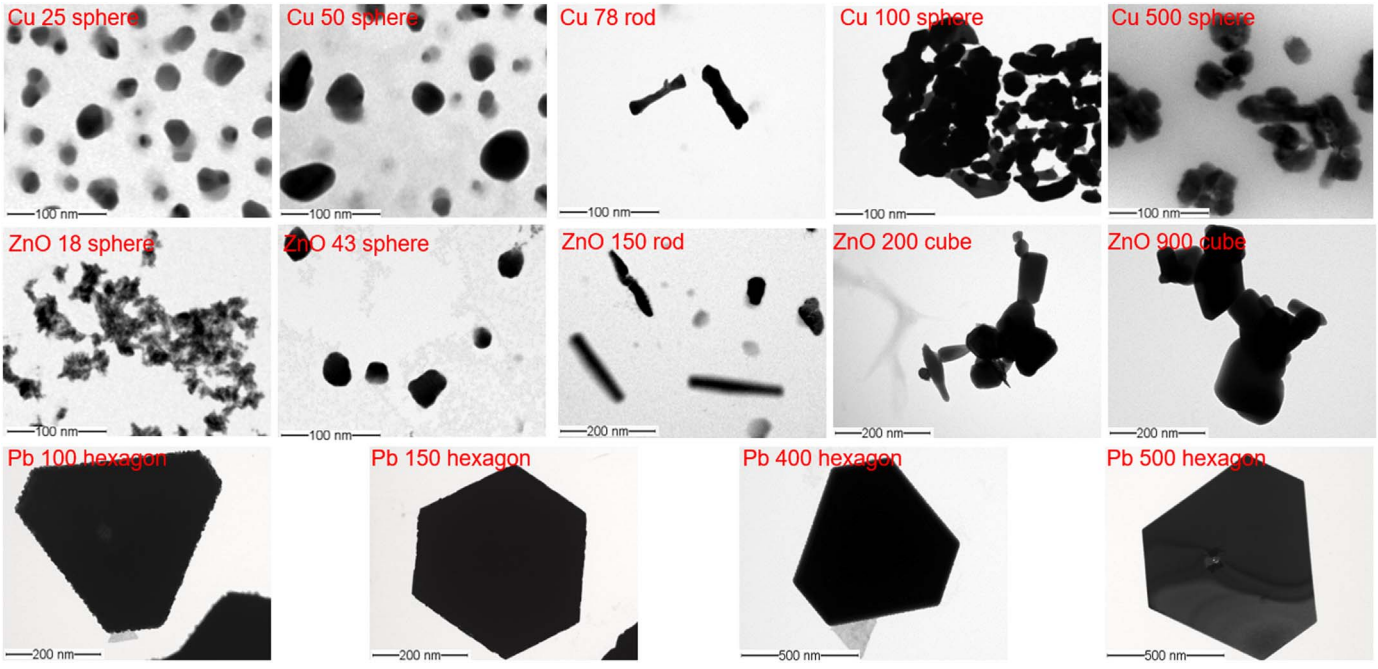

Fig. 1. Transmission electron microscopic images of ENMs and SMPs in the exposure medium.

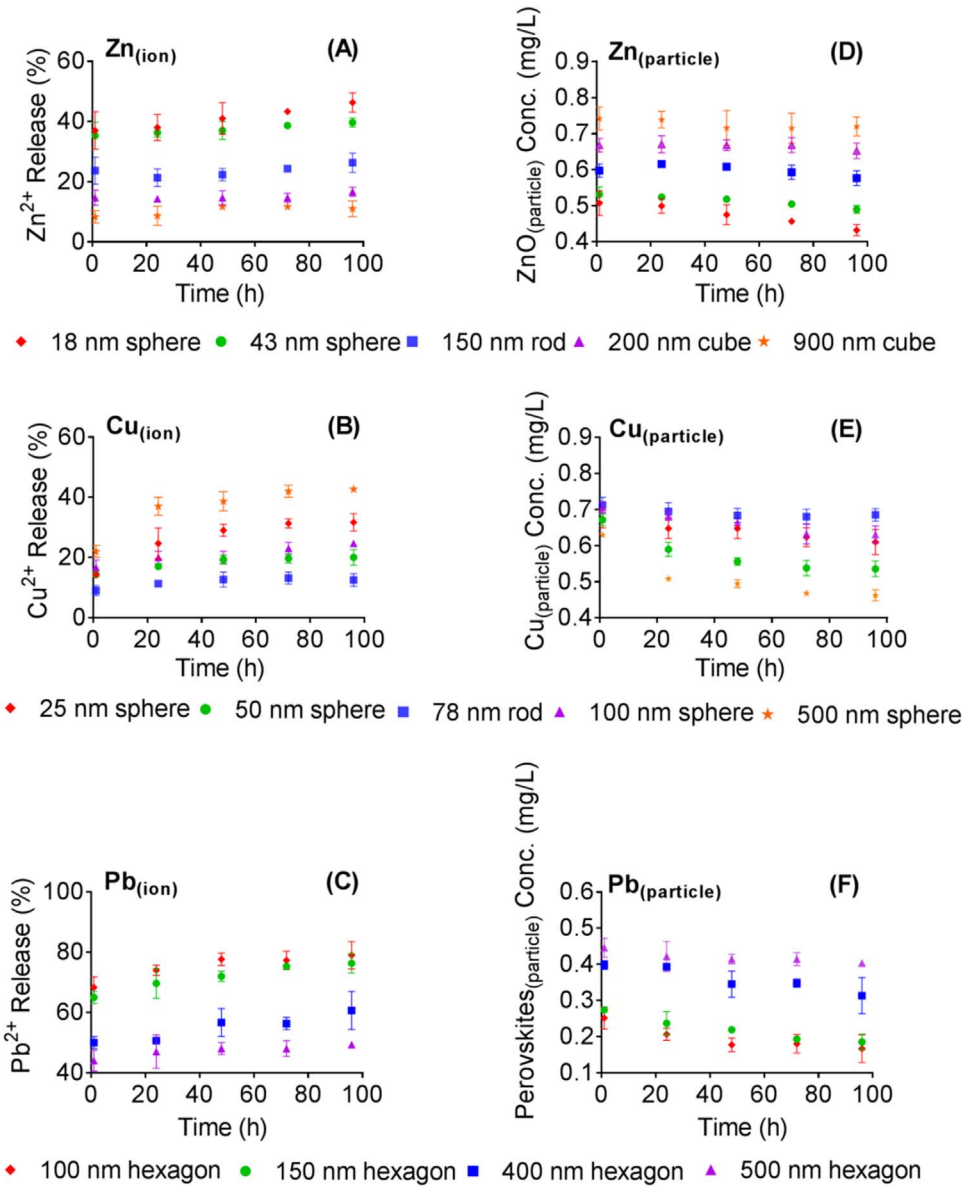

Fig. 2. Ion release profiles and concentrations of particulate forms of 1 mg/L ENMs and SMPs suspensions, during 96 h in the exposure medium. (A) Relative percentage of dissolved Zn released from nano-ZnO and SMPs. (B) Relative percentage of dissolved Cu released from nano-Cu and SMPs. (C) Relative percentage of dissolved Pb released from Perovskites. (D) Zn concentrations of the nano-ZnO and $SMPs_{(particle)}$. (E) Cu concentrations of the nano-Cu and $SMPs_{(particle)}$. (F) Pb concentrations of the $perovskites_{(particle)}$. Data are mean ± SD (n = 3).

incubation, the concentrations of spherical 25–100 nm nano-$Cu_{(particle)}$ were 9–17% less than the initial concentrations. However, the decrease of the concentrations of 500 nm spherical Cu $SMP_{(particle)}$ (26%) was higher than the concentrations of rod-shaped 78 nm nano-$Cu_{(particle)}$ (4%), which was due to the higher ion release of spherical 500 nm Cu SMP than the rod-shaped 78 nm nano-Cu (Fig. 2E). The decrease of the concentration of $perovskites_{(particle)}$ was even higher, up to 13–37% after 96 h, depending on the size of the particles (Fig. 2F).

3.3. Responses of bacterial communities following exposure to ENMs and SMPs

The dose-response curves of suspensions of ENMs and SMPs and their corresponding metal salts are provided in Fig. 3 (A-C), in which the response was expressed as average well color development (AWCD) values of Ecoplates in proportion to the control. The metabolic potential of soil bacterial communities decreased with increasing concentrations of ENMs and SMPs suspensions and their corresponding metal salts. The total concentrations of suspensions of ENMs and SMPs causing 50% inhibition of bacterial activity (EC_{50}) are listed in Table 1. The EC_{50} values of $Zn(NO_3)_2{\cdot}6H_2O$, $CuCl_2{\cdot}2H_2O$, and $PbCl_2$ were 0.95, 0.16 and 5.26 mg/L, respectively, as based on the metal ion concentrations which were lower than those of the corresponding ENMs and SMPs, indicating that Zn(II), Cu(II) and Pb(II) are the most toxic of all the tested chemicals. The dose-response curves of the particulate forms of ENMs and SMPs based on the RA model are provided in Fig. 3 (D-F). The EC_{50} values of particulate forms of ENMs and SMPs using the response addition model (RA) are shown in Table 1. After comparting the EC_{50} values of different metal type of ENMs and SMPs, nano-Cu and $SMPs_{(particle)}$ were found to be the most toxic of the particles tested (0.28–0.74 mg/L), followed by nano-ZnO and $SMPs_{(particle)}$ (1.07–2.09 mg/L), and $perovskites_{(particle)}$ (25.31–74.57 mg/L). Comparing the EC_{50} values of the same metal type of ENMs and SMPs with different shapes and sizes, the spherical 18–43 nm nano-$ZnO_{(particle)}$ had lower EC_{50} values (1.07–1.52 mg/L) than the rod-shaped 150 nm and cuboidal 200–900 nm ZnO $SMPs_{(particle)}$ (2.06–2.17 mg/L) (Fig. 3D). The EC_{50} values of spherical 25–100 nm nano-$Cu_{(particle)}$ (0.28–0.56 mg/L) were lower than the rod-shaped 78 nm nano-$Cu_{(particle)}$ (0.74 mg/L) (Fig. 3E). Depending on the different shapes of the same type of ENMs and SMPs, spherical particles were found to be the most toxic among all the tested particles, followed by rod and polygonal shaped particles. Smaller sized particles of ZnO and

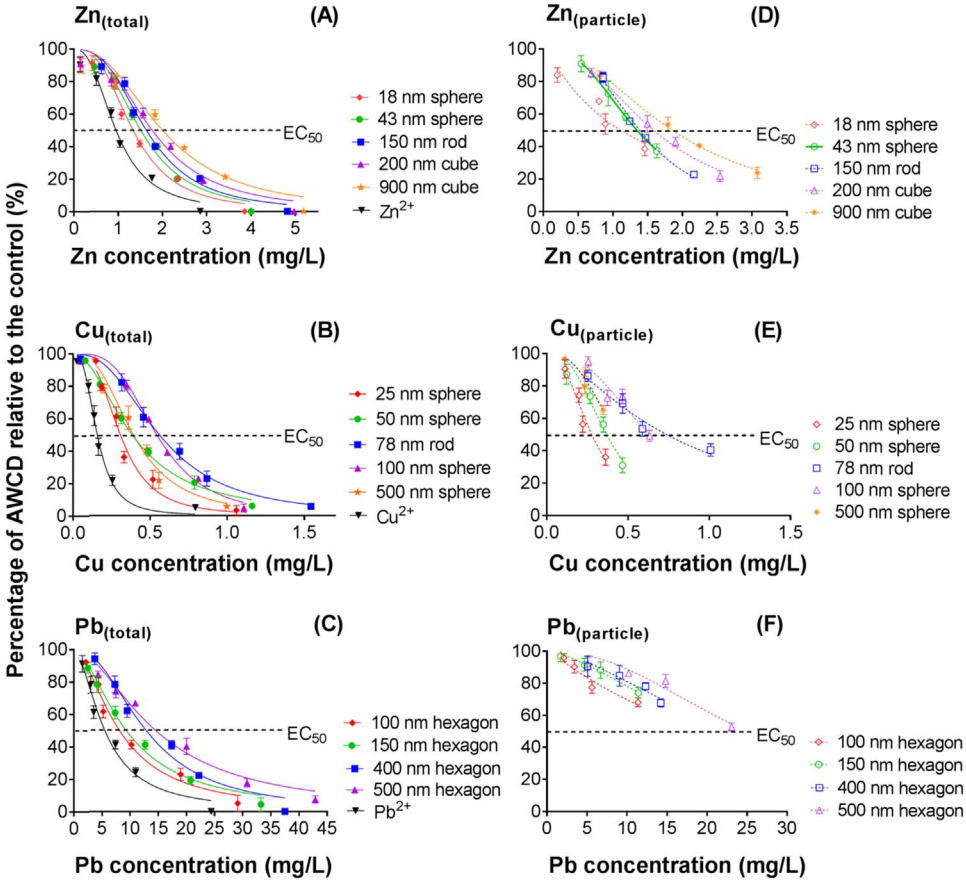

Fig. 3. Dose-response curves of AWCD of soil extracts exposed to ENMs and SMPs suspensions of (A) nano-ZnO, $SMPs_{(total)}$ and $Zn(NO_3)_2{*}6H_2O$, (B) nano-$Cu_{(total)}$, SMPs and $CuCl_2{*}2H_2O$, (C) $perovskites_{(total)}$ and $PbCl_2$, (D) nano-ZnO and $SMPs_{(particle)}$, (E) CuNPs and $SMPs_{(particle)}$, and (F) $perovskites_{(particle)}$. AWCD values relative to the control are plotted on the y-axis, actual log-transformed metal concentrations are plotted on the x-axis. Data are mean ± SD (n = 3).

perovskites with the same shape were found to be more toxic than larger sizes (Fig. 3 F). However, the EC_{50} value of spherical 500 nm Cu SMPs (0.45 mg/L) was lower than the EC_{50} value of rod-shaped 78 nm nano-Cu (0.74 mg/L), which was due to the morphology according to the TEM observation that rough surface of 500 nm Cu SMPs may cause fast decomposition of the particles.

In addition, The EC_{50} values of particulate forms of ENMs and SMPs based on initial measured concentrations (C_I) and TWA concentrations (C_{TWA}) are also listed in Table 1. The EC_{50} values of spherical nano-ZnO were significantly lower when expressed as C_{TWA} compared to the EC_{50} values expressed as C_I ($p < 0.05$), and the use of C_{TWA} significantly reduced the EC_{50} values of spherical nano-Cu and SMPs ($p < 0.05$). The EC_{50} values of all the perovskites also decreased significantly after being corrected using the TWA approach ($p < 0.05$), which can be explained by the highest extent of dissolution observed for perovskites amongst all tested ENMs and SMPs.

The relative contributions of the particulate forms and the ionic forms of ENMs and SMPs to the overall toxicity of the suspensions of ENMs and SMPs to bacterial communities at the EC_{50} level based on the RA model are given in Table 2. The 150–900 nm ZnO $SMPs_{(particle)}$ significantly contributed to the overall toxicity of all the zinc suspensions (84–96%). Although the EC_{50} of Zn(II) in $Zn(NO_3)_2$ (0.95 mg/L) was found to be lower than the EC_{50} values of the nano-ZnO and SMPs (1.34–1.99 mg/L), the high contribution of ZnO $SMPs_{(particle)}$ was ascribed to the low level of released Zn ion. However, the relative contribution of nano-Cu and $SMPs_{(particle)}$ was dependent on the ion release profiles. The particulate forms only significantly contributed to the total response in the bacterial communities that were exposed to 78 nm rod-shaped nano-Cu (67%). The EC_{50} of Cu(II) in $CuCl_2$ (0.16 mg/L) was less than half of the values of the nano-Cu and SMPs (0.30–0.57 mg/L). The ionic forms exhibited higher toxicity than the particle forms to the overall response when bacterial communities exposed to 25 nm nano-Cu (60%) and 500 nm spherical Cu SMPs (76%) because of the high levels of Cu ions released in the suspensions and high toxicity of Cu ions. The ionic forms of perovskites showed high contributions to the overall response of the bacterial communities in all cases. This was due to the high toxicity of Pb(II) in $PbCl_2$ and high level of Pb ions released from perovskites.

Table 2
Comparison of relative toxic contributions of ion and the particulate form of ENMs and SMPs to toxicity at the EC_{50} level based on C_{TWA} using the RA model.

Element	Size and shape	Relative toxic contribution	
		Ion	particle
Zn	18 nm spheres[a]	41	59
	43 nm spheres[a]	47	53
	150 nm rods[b]	16	84
	200 nm cubes[b]	7	93
	900 nm cubes[b]	4	96
Cu	25 nm spheres[a]	60	40
	50 nm spheres[a]	52	48
	78 nm rods[a]	33	67
	100 nm spheres[a]	50	50
	500 nm spheres[b]	76	23
Pb	100 nm hexagon[a]	81	19
	150 nm hexagon[b]	84	16
	400 nm hexagon[b]	74	26
	500 nm hexagon[b]	76	24

[a] Nano particles (ENMs).
[b] Submicron particles (SMPs).

3.4. Bacterial utilization of environmentally relevant carbon substrates

The changes of functional potential of bacterial communities were explored to further explain the toxicity of ENMs and SMPs. The capacity

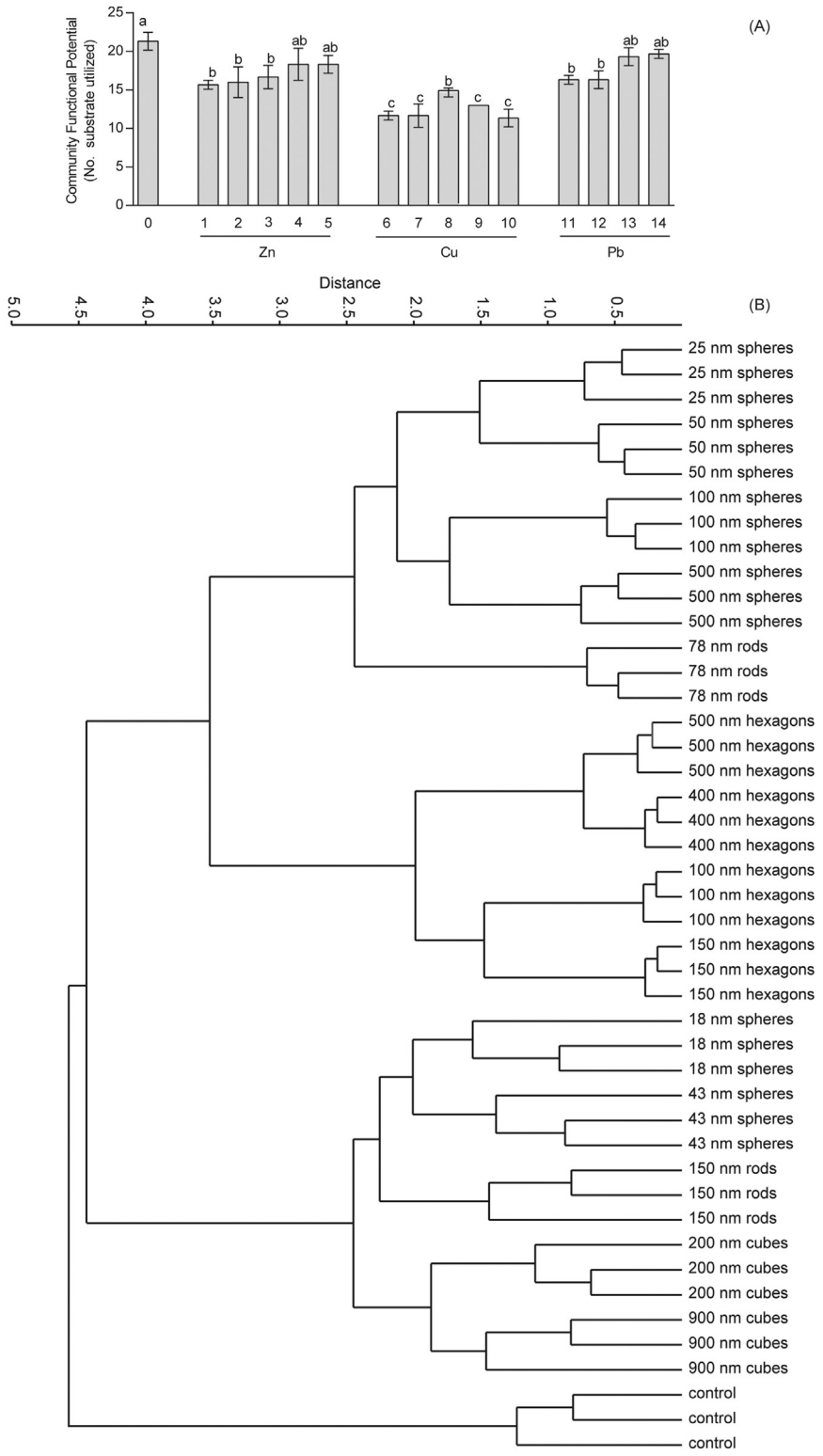

Fig. 4. Functional potential of bacterial communities under different ENMs and SMPs treatments at EC_{50} level. (A) Utilization of carbon substrates by bacterial communities exposed to different ENMs and SMPs. The bars are the mean ± SD (representative experiment showing n = 3 in triplicates). The different letters indicate significant differences between each treatment and control by a two-way ANOVA and Tukey's honestly significant difference tests (with significance level set as $p < 0.05$). (0 = control, 1 = 18 nm spheres, 2 = 43 nm spheres, 3 = 150 nm rods, 4 = 200 nm cubes, 5 = 900 nm cubes; 6 = 25 nm spheres, 7 = 50 nm spheres, 8 = 78 nm rods, 9 = 100 nm spheres, 10 = 400 nm spheres; 11 = 100 nm hexagon, 12 = 150 nm hexagon, 13 = 400 nm hexagon, 14 = 500 nm hexagon). (B) Classifications of different ENMs and SMPs treatments by cluster analysis according to the AWCD of the bacterial communities at EC_{50} level. (one-way ANOSIM, Euclidean-based similarity, n = 3, $R^2 = 0.996$, $p < 0.05$).

of the bacterial communities to utilize different carbon sources following exposure to nano-ZnO and SMPs, nano-Cu and SMPs, and perovskites treatments at the EC_{50} level is shown in Fig. 4(A). Patterns in carbon substrate utilization reflected differences in the substrates utilizations of the bacterial communities among different ENMs and SMPs treatments at the EC_{50} level (Fig. A.1). The exposure to ENMs and SMPs reduced the community functional potential. Compared to the control, treatments of spherical and rod-shaped nano-ZnO and SMPs significantly reduced the number of substrate utilizations ($p < 0.05$). For nano-Cu and SMPs, the functional potential under plate and spherical particles treatments was significantly lower than in case of treatment with rod-shaped particles ($p < 0.05$). For perovskites, the exposure to 100 and 150 nm significantly inhibited the substrate utilization of bacterial communities ($p < 0.05$).

Classifications of different nano-ZnO and SMPs, nano-Cu and SMPs, and perovskites treatments by cluster analysis according to the

metabolic characteristics of the bacterial communities at the EC_{50} level are presented in Fig. 4(B). The bacterial functional potential differed significantly between treatments depending on the element of the metal-based particles (one-way ANOSIM: $R = 0.996$, $p < 0.05$). The metabolic characteristics of the bacterial communities was also analyzed using principal component analysis (PCA) at the EC_{50} level (Fig. A.2). The PCA plots indicated that metabolic profiles from the ENMs and SMPs distinguished from that of the control. The treatments of same metal type of ENMs and SMPs closely-grouped, indicating similar bacterial functional potential.

4. Discussion

The results of this study showed that ENMs significantly affect soil bacterial community and functional potential. Particle dissolution is affected by the physico-chemical characteristics of ENMs, e.g. shape, size, and initial concentration (Wang et al., 2012). Here we assessed ENMs differing in dissolution potential. The spherical nano-ZnO and -Cu were demonstrated to be more soluble than the other shapes of ENMs of the same chemical composition in the exposure medium, and the ion release of rod-shaped nano-Cu and cuboidal ZnO SMPs were the lowest. From the assessment of the dissolution behavior of ENMs in the exposure medium we also found that the exposure concentrations for the particulate forms of ENMs declined along with time (Fig. 3 D-F). To account for these dynamics in dissolution we expressed the exposure concentrations of ENMs based on TWA. This is assumed to be a more accurate and naturally relevant description of effects and risks compared to those expressed by initially measured concentrations during the different exposure periods. The TWA approach has been applied for the macrophyte *Myriophyllum spicatum* and exposure to the herbicide metsulfuron-methyl (Belgers et al., 2011). In our study, the EC_{50} values of spherical nano-ZnO and -Cu as well as perovskites based on TWA approach were significantly lower than those based on initially measured concentrations.

In determining the relative contributions of the particulate forms and the ionic forms to ENMs-toxicity, concentration addition (CA) model and response addition (RA) model are widely used to predict the joint toxicity of chemicals in a mixture based on their individual effects. Since the CA model acts independently of the mechanism of action, and therefore has the tendency to be conservative (Gregorio et al., 2013), and the majority of studies focused on models that assume dissimilar mechanisms of action driving mixture toxicity (Altenburger et al., 2003), we applied the response addition model to compare effects of the particulate forms and the ionic forms of ENMs. (Table 1). Our results showed that at the EC_{50} level, both the particulate forms and ionic forms of spherical nano-ZnO and nano-Cu are responsible for changing the functional potential of soil bacterial communities (Table 2). Noteworthy, the ionic form of perovskites contributes far more than the particulate forms, and Cu ions also contributed significantly when bacterial communities were exposed to 25 nm nano-Cu and 500 nm SMPs. Toxicity caused by the ionic metal species has been reported with spherical 2.8–10.5 nm nano-Ag on *Escherichia coli* (Xiu et al., 2012), 20 nm nano-ZnO on *Saccharomyces cerevisiae* (Zhang et al., 2016), *pseudokirchneriella subcapitata* (Franklin et al., 2007), and nano-Ag on HeLa and A549 cells (De Matteis et al., 2015), including membrane damage, mitochondrial damage, oxidative stress (ROS) and lipid peroxidation (Ivask et al., 2014). However, our results also showed that the relative contributions of the particulate forms to toxicity were much higher than those of the ionic forms in suspensions of ZnO SMPs and rod-shaped 78 nm nano-Cu. These results are in concurrence with the previous work of Bhuvaneshwari et al. (2016), showing that the contributions from 50 and 100 nm nano-$ZnO_{(particle)}$ to the overall toxicity to *Ceriodaphnia dubia* were notable. Similarly, Sun et al. (2017) also found that the particles rather than the dissolved ions were the dominant source of nano-CuO toxicity to the hemocytes of *Chlamys farreri*. Taken together, the physico-chemical properties like metal type, shape, size, dissolution and stability/aggregation of ENMs can affect the contributions of particulate forms and ionic forms to the overall response. The size-dependent and shape-dependent toxicity of ENMs were due to the surface-to-volume ratio of the particles, and the direct contact area with cells (Hua et al., 2014; Simon-Deckers et al., 2009). The dissolution and stability/aggregation of ENMs also caused time-response DNA damage in cells exposed to $ENMs_{(particle)}$ and $ENMs_{(ion)}$ (Gomes et al., 2013). On the one hand, the antibacterial activity of ENMs might related to the released metal ions (Hajipour et al., 2013). On the other hand, The $ENMs_{(particle)}$ could also enter the cell to generate ROS and inhibited the proliferation of cells (McShan et al., 2014), indicating that a particle-mediated mechanism also promoted the contribution of $ENMs_{(particle)}$ to the overall toxicity.

Toxicity studies of ENMs of different composition have been performed on a variety of species with different sizes and shapes. In our study, the EC_{50} values of nano-ZnO and SMPs and perovskites were size dependent, whereby smaller sized particles showed higher toxicity. The size-effect of ENMs has previously been described with daphnids (Lopes et al., 2014), algae (Aruoja et al., 2009) and bacteria (Simon-Deckers et al., 2009). However, our results also showed that spherical 500 nm Cu SMPs were more toxic than rod-shaped 78 nm nano-Cu, which was due to the morphology and dissolution of particles according to the TEM observation and ion release profiles. The rough surface of 500 nm Cu SMPs may cause fast decomposition of the particles. Therefore, the size of 500 nm Cu SMPs in the media was found to be decreased as the net surface area and dissolution of SMPs increased (Song et al., 2015). The shapes of nano-ZnO and -Cu were found to influent their toxicity to mammalian and piscine cell lines, daphnia and zebrafish embryos (Xiao et al., 2015; Song et al., 2014; Hua et al., 2014). In our present study, compared with the other spherical nano-ZnO and -Cu, the rod-shaped 150 nm ZnO SMPs and 78 nm nano-Cu were less toxic (Figs. 3B and 3 C). These findings with regard to the stability and low toxicity of rod-shaped ENMs are consistent with previous findings, with net surface area of rod-shaped particles being much smaller compared with spherical ENMs (Song et al., 2015). For Perovskites, the ABX_3 crystal structure and chemical reactions of perovskites in the aqueous phase can lead to the release of Pb ions and subsequent toxic effects on soil bacterial communities. Furthermore, our results showed that the utilization of carbon sources by bacterial communities was inhibited after exposure to ENMs (Fig. 4A), indicating that the bacterial functional potential was negatively affected (Echavarri-Bravo et al., 2015). The bacterial functional potential differed significantly between treatments depending on the tested metal (Fig. 4B). These findings indicate that ENMs do bring additional nano-specific effects, with the structure and ion release of ENMs being two of the important factors that need to be considered when investigating the toxicity profiles of ENMs.

Not accounting for environmental chemistry (e.g. pH, temperature, biofilms, humic acids) that can affect the toxicity of ENMs, our results thus should be interpreted cautiously. It is also uncertain whether patterns observed in this study reflect exposure dynamics of ENMs in natural systems. However, the effect of dissolution and aggregation dynamics of ENMs on the metabolic potential of soil bacterial community are likely relevant in natural environments. Our results thus hint that the time-variable exposures of ENMs can disrupt metabolic processes of natural soil bacterial communities and in turn their associated ecosystem processes, warranting consideration of the dynamic exposure of ENMs. The assessment of environmentally relevant risks and biochemical interactions with ENMs effects on bacterial communities are therefore promising areas of future research.

5. Conclusions

This study evaluated the effect of three different types of metal-based ENMs that differ in size, shape and dissolution potential on the metabolic potential of soil bacterial communities. The EC_{50} values of spherical nano-ZnO, spherical nano-Cu and SMPs, and Pb-based

perovskites were shown to be significantly lower based on time weighted average concentrations compared to responses derived from the traditional approach relying on a constant initial concentration. In addition, both particulate forms and ionic forms of spherical 18, 43 nm nano-ZnO and 50 nm, 100 nm nano-Cu contributed to the overall response at the EC_{50} levels. The particulate forms for 150 nm, 200 nm and 900 nm ZnO SMPs and rod-shaped 78 nm nano-Cu were the dominant factors governing soil bacterial community utilization carbon substrates, or metabolic potential. Contrarily, the Cu ions released from spherical 25 nm nano-Cu, 500 nm Cu SMPs and Pb ions released from perovskites were driving soil bacterial community metabolic potential. Taken together, our findings underlined that the effect caused by particles and ionic forms of ENMs can only be reliably assessed when physico-chemical properties e.g. size, dissolution and stability/aggregation are taken into account. Although the realistic exposure scenarios cannot be completely reflected by the results obtained in substrate utilization, our findings represent the basis for a better understanding the effects of ENMs on the catabolic potential of bacterial communities. This outcome thus presents a case to consider exposure dynamics and relative contributions of both particulate form and ions shedding from ENMs to better understand potential risks of ENMs and to allow for a more a conservative and realistic environmental risk assessment.

Acknowledgements

The research described in this work was supported by the European Union Seventh Framework Programme under EC-GA 'FUTURENANONEEDS' [project number 604602]. The Chinese Scholarship Council (CSC) is gratefully acknowledged for its financial support to Yujia Zhai [201506510003]. Martina G. Vijver is funded by NWO-VIDI [project number 864.13.010].

Appendix A. Supplementary material

Supplementary data associated with this article can be found in the online version at http://dx.doi.org/10.1016/j.ecoenv.2017.07.031.

References

Altenburger, R., Nendza, M., Schuurmann, G., 2003. Mixture toxicity and its modeling by quantitative structure–activity relationships. Environ. Toxicol. Chem. 22, 1900–1915.

Aruoja, V., Dubourguier, H.-C., Kasemets, K., Kahru, A., 2009. Toxicity of nanoparticles of CuO, ZnO and TiO_2 to microalgae *Pseudokirchneriella subcapitata*. Sci. Total Environ. 407, 1461–1468.

Backhaus, T., Scholze, M., Grimme, L., 2000. The single substance and mixture toxicity of quinolones to the bioluminescent bacterium Vibrio fischeri. Aquat. Toxicol. 49, 49–61.

Belgers, J.D.M., Aalderink, G.H., Arts, G.H.P., Brock, T.C.M., 2011. Can time-weighted average concentrations be used to assess the risks of metsulfuron-methyl to Myriophyllum spicatum under different time-variable exposure regimes? Chemosphere 85, 1017–1025.

Bhuvaneshwari, M., Iswarya, V., Nagarajan, R., Chandrasekaran, N., Mukherjee, Amitava, 2016. Acute toxicity and accumulation of ZnO NPs in *Ceriodaphnia dubia*: relative contributions of dissolved ions and particles. Aquat. Toxicol. 177, 494–502.

Bloem, J., Bolhuis, P.R., 2006. Thymidine and leucine incorporation to assess bacterial growth rate. In: Bloem, J., Benedetti, A., Hopkins, D.W. (Eds.), Microbiological Methods for Assessing Soil Quality. CABI, Wallingford, UK, pp. 142–149.

Boudreau, M.D., Imam, M.S., Paredes, A.M., Bryant, M.S., Cunningham, C.K., Felton, R.P., Jones, M.Y., Davis, K.J., Olson, G.R., 2016. Differential effects of silver nanoparticles and silver ions on tissue accumulation, distribution, and toxicity in the Sprague Dawley rat following daily oral gavage administration for 13 weeks. Toxicol. Sci. 150, 130–160.

De Matteis, V., Malvindi, M.A., Galeone, A., Brunetti, V., De Luca, E., Kote, S., Kshirsagar, P., Sabella, S., Bardi, G., Pompa, P.P., 2015. Negligible particle-specific toxicity mechanism of silver nanoparticles: the role of Ag^+ ion release in the cytosol. Nanomed.: Nanotechnol., Biol. Med. 11 (3), 731–739.

Du, L., Arnholt, K., Ripp, S.A., Sayler, G.S., Wang, S., Zhuang, J., 2015. Biological toxicity of cellulose nanocrystals (CNCs) against the luxCDABE-based bioluminescent bioreporter *Escherichia coli* 652T7. Ecotoxicology 24 (10), 2049–2053.

Echavarri-Bravo, V., Paterson, L., Aspray, T.J., Porter, J.S., Winson, M.K., Thornton, B., Hartl, M.G.J., 2015. Shifts in the metabolic function of a benthic estuarine microbial community following a single pulse exposure to silver nanoparticles. Environ. Pollut. 201, 91–99.

Franklin, N.M., Rogers, N.J., Apte, S.C., Batley, G.E., Gadd, G.E., Casey, P.S., 2007. Comparative toxicity of nanoparticulate ZnO, bulk ZnO, and $ZnCl_2$ to a freshwater microalga (*Pseudokirchneriella subcapitata*): the importance of particle solubility. Environ. Sci. Technol. 41, 8484–8490.

Garland, J.L., Mills, A.L., 1991. Classification and characterization of heterotrophic microbial communities on the basis of patterns of community-level sole-carbon-source utilization. Appl. Environ. Microbiol. 57, 2351–2359.

Gomes, T., Araújo, O., Pereira, R., Almeida, A.C., Cravo, A., Bebianno, M.J., 2013. Genotoxicity of copper oxide and silver nanoparticles in the mussel *Mytilus galloprovincialis*. Mar. Environ. Res. 84, 51–59.

Gregorio, V., Chèvre, N., Junghans, M., 2013. Critical issues in using the common mixture toxicity models concentration addition or response addition on species sensitivity distributions: a theoretical approach. Environ. Toxicol. Chem. 32 (10), 2387–2395.

Hajipour, M.J., Fromm, K.M., Ashkarran, A.A., de Aberasturi, D.J., de Larramendi, I.R., Rojo, T., Serpooshan, V., Parak, W.J., Mahmoudi, M., 2013. Antibacterial properties of nanoparticles. Trends Biotechnol. 31 (1), 612–662.

Hammer, Ø., Harper, D.A.T., Ryan, P.D., 2001. PAST: paleontological statistics software package for education and data analysis. Palaeontol. Electron. 4, 9.

Hua, J., Vijver, M.G., Richardson, M.K., Ahmad, F., Peijnenburg, W.J., 2014. Particle-specific toxic effects of differently shaped zinc oxide nanoparticles to zebrafish embryos (*Danio rerio*). Environ. Toxicol. Chem. 33, 2859–2868.

Hunting, E.R., White, C.M., van Gemert, M., Mes, D., Stam, E., van der Geest, H.G., Kraak, M.H.S., Admiraal, W., 2013. UV radiation and organic matter composition shape bacterial functional diversity in sediments. Front. Microbiol. 4, 317.

Hunting, E.R., Vijver, M.G., van der Geest, H.G., Mulder, C., Kraak, M.H.S., Breure, A.M., Admiraal, W., 2015. Resource niche overlap promotes stability of bacterial community metabolism in experimental microcosms. Front. Microbiol. 6, 105.

Ivask, A., Juganson, K., Bondarenko, O., Mortimer, M., Aruoja, V., Kasemets, K., Blinova, I., Heinlaan, M., Slaveykova, V., Kahru, A., 2014. Mechanisms of toxic action of Ag, ZnO and CuO nanoparticles to selected ecotoxicological test organisms and mammalian cells in vitro: a comparative review. Nanotoxicology 8, 57–71.

Karlsson, H.L., Cronholm, P., Gustafsson, J., Moller, L., 2008. Copper oxide nanoparticles are highly toxic: a comparison between metal oxide nanoparticles and carbon nanotubes. Chem. Reserch Toxicol. 21 (9), 1726–1732.

Kermanizadeh, A., Gaiser, B.K., Hutchison, G.H., Stone, V., 2012. An in vitro liver model-assessing oxidative stress and genotoxicity following exposure of hepatocytes to a panel of engineered nanomaterials. Part. Fibre Toxicol. 9, 28.

Lopes, S., Ribeiro, F., Wojnarowicz, J., Łojkowski, W., Jurkschat, K., Crossley, A., Soares, A.M., Loureiro, S., 2014. Zinc oxide nanoparticles toxicity to *Daphnia magna*: size-dependent effects and dissolution. Environ. Toxicol. Chem. 33, 190–198.

McShan, D., Ray, P.C., Yu, H., 2014. Molecular toxicity mechanism of nanosilver. J. Food Drug Anal. 22 (1), 116–127.

McKee, M.S., Filser, J., 2016. Impacts of metal-based engineered nanomaterials on soil communities. Environ. Sci.: Nano 3, 506–533.

Meesters, J.A.J., Veltman, K., Hendriks, A.J., van de Meent, D., 2013. Environmental exposure assessment of engineered nanoparticles: why REACH needs adjustment. Environ. Monit. Assess. 9, 15–26.

Misra, S.K., Dybowska, A., Berhanu, D., Luoma, S.N., Valsami-Jones, E., 2012. The complexity of nanoparticle dissolution and its importance in nanotoxicological studies. Sci. Total Environ. 438, 225–232.

Rutgers, M., Wouterse, M., Drost, S.M., Breure, A.M., Mulder, C., Stone, D., Creamer, R.E., Winding, A., Bloem, J., 2016. Monitoring soil bacteria with community-level physiological profiles using Biolog™ ECO-plates in the Netherlands and Europe. Appl. Soil Ecol. 97, 23–35.

Rutgers, M., Breure, A.M., Insam, H., 2006. 8.4. Substrate utilization in BiologTMplatesfor analysis of CLPP. In: Bloem, J., Benedetti, A., Hopkins, D.W. (Eds.), Microbiological Methods for Assessing Soil Quality. CABI, Wallingford, Oxfordshire, UK, pp. 212–227.

Santo, N., Fascio, U., Torres, F., Guazzoni, N., Tremolada, P., Bettinetti, R., Mantecca, P., Bacchetta, R., 2014. Toxic effects and ultrastructural damages to *Daphnia magna* of two differently sized ZnO nanoparticles: does size matter? Water Res. 53, 339–350.

Schutter, M., Dick, R., 2001. Shifts in substrate utilization potential and structure of soil microbial communities in response to carbon substrates. Soil Biol. Biochem. 33 (11), 1481–1491.

Shah, V., Belozerova, I., 2009. Influence of metal nanoparticles on the soil microbial community and germination of lettuce seeds. Water, Air, Soil Pollut. 197, 143–148.

Sillen, W.M.A., Thijs, S., Abbamondi, G.R., Janssen, J., Weyens, N., White, J.C., Vangronsveld, J., 2015. Effects of silver nanoparticles on soil microorganisms and maize biomass are linked in the rhizosphere. Soil Biol. Biochem. 91, 14–22.

Simon-Deckers, A., Loo, S., Mayne-L'Hermite, M., Herline-Boime, N., Menguy, N., Reynaud, C., Gouget, B., Carriere, M., 2009. Size-, Composition- and Shape-Dependent Toxicological Impact of Metal Oxide Nanoparticles and Carbon Nanotubes toward Bacteria. Environ. Sci. Technol. 43, 8423–8429.

Stefanowicz, A., 2006. The biolog plates technique as a tool in ecological studies of microbial communities. Pol. J. Environ. Stud. 15, 669–676.

Song, L., Connolly, M., Fernández-Cruz, M.L., Vijver, M.G., Fernández, M., Conde, E., de Snoo, G.R., Peijnenburg, W.J.G.M., Navas, J.M., 2014. Species-specific toxicity of copper nanoparticles among mammalian and piscine cell lines. Nanotoxicology 8, 383–393.

Song, L., Vijver, M.G., de Snoo, G.R., Peijnenburg, W.J., 2015. Assessing toxicity of copper nanoparticles across five cladoceran species. Environ. Toxicol. Chem. 34, 1863–1869.

Sun, X., Chen, B., Xia, B., Han, Q., Zhu, Lin, Qua, K., 2017. Are CuO nanoparticles effects on hemocytes of the marine scallop (Chlamys farreri) caused by particles and/or corresponding released ions? Ecotoxicol. Environ. Saf. 139, 65–72.

Topuz, E., van Gestel, C.A.M., 2015. Toxicodynamics and toxicodynamics of differently

coated silver nanoparticles and silver nitrate in *Enchytraeus crypticus* upon aqueous exposure in an inert sand medium. Environ. Toxicol. Chem. 34, 2816–2823.
Villéger, S., Mason, N.W.H., Mouillot, D., 2008. New multidimensional functional diversity indices for a multifaceted framework in functional ecology. Ecology 89, 2290–2301.
Wang, T., Zhang, D., Dai, L., Chen, Y., Dai, X., 2016. Effects of metal nanoparticles on methane production from waste-activated sludge and microorganism community shift in anaerobic granular sludge. Sci. Rep. 6, 25857.
Wang, Z., Chen, J., Li, X., Shao, J., Peijnenburg, W.J.G.M., 2012. Aquatic toxicity of nanosilver colloids to different trophic organisms: contributions of particles and free silver ion. Environ. Toxicol. Chem. 31, 2408–2413.
Weber, K.P., Grove, J.A., Gehder, M., Anderson, W.A., Legge, R.L., 2007. Data transformations in the analysis of community-level substrate utilization data from microplates. J. Microbiol. Methods 69, 461–469.
Xiao, Y., Vijver, M.G., Chen, G., Peijnenburg, W.J.G.M., 2015. Toxicity and accumulation of Cu and ZnO nanoparticles in *Daphnia magna*. Environ. Sci. Technol. 49, 4657–4664.
Xiu, Z., Zhang, Q., Puppala, H.L., Colvin, V.L., Alvarez, P.J.J., 2012. Negligible particle-specific antibacterial activity of silver nanoparticles. Nano Lett. 12, 4271–4275.
Zhang, W., Liu, X., Bao, S., Xiao, B., Fang, T., 2016. Evaluation of nano-specific toxicity of zinc oxide, copper oxide, and silver nanoparticles through toxic ratio. J. Nanopart. Res. 18, 372.
Zhai, Y., Hunting, E.R., Wouters, M., Peijnenburg, W.J.G.M., Vijver, M.G., 2016. Silver nanoparticles, ions, and shape governing soil microbial functional diversity: nano shapes micro. Front. Microbiol. 7, 1123.